Central European Journal of Energetic Materials
ISSN 1733-7178; e-ISSN 2353-1843

Cent. Eur. J. Energ. Mater. 2017, *14*(4): 788-805; DOI: 10.22211/cejem/78753

Enhanced Non-linear Viscoelastic Properties of Polymer Bonded Explosives Based on Graphene and a Neutral Polymeric Bonding Agent

Congmei Lin,[1,2*] Guansong He,[1] Jiahui Liu,[1] Liping Pan,[1] Shijun Liu [1]

[1] *Institute of Chemical Materials, CAEP, Mianshan Load 64#, 621900 Mianyang, China*
[2] *The State Key Laboratory of Polymer Materials Engineering, Polymer Research Institute of Sichuan University, 610065 Chengdu, China*
[*] *E-mail: lincmei2009@caep.cn*

Abstract: During their long-term storage and transport, polymer bonded explosives (PBXs) will be subjected to complex thermal physical environments with combined thermal and mechanical loads. The creep behaviour results in a change of physical and mechanical properties, which consequently influences the explosive performance. In this work, graphene and a neutral polymeric bonding agent (NPBA) were selected to improve the non-linear creep properties of 1,3,5-triamino-2,4,6-trinitrobenzene (TATB)-based PBXs. The results were compared with the creep response of the corresponding PBXs without additives and with graphene alone. It was observed that graphene and an NPBA exhibited a positive effect, improving the creep resistance of TATB-based PBXs. The compressive and tensile strength of 0.5 wt.% graphene-filled PBXs were improved by 5.1% and 29.2%, respectively, compared to raw TATB-based PBXs without additives. The performance of the PBXs was further enhanced by the addition of 0.1 wt.% NPBA. For a given stress and temperature, the TATB-based PBXs with graphene and NPBA deformed significantly less than the PBXs filled with graphene alone.

Keywords: polymer bonded explosives, graphene, neutral polymeric bonding agent, creep behaviour

1 Introduction

Due to the exceptional thermal, mechanical, and electrical properties of graphene, it is of great interest to academia and industry as a nano-filler in composite materials [1-7]. The thermal conductivity and mechanical stiffness of graphene are 3000 W/(m·K) and 1060 GPa, respectively [8]. Therefore, graphene has been extensively applied as a conductive or mechanical modifier in polymeric composites. It has been revealed that graphene sheets also have extraordinary electronic transport properties [9].

A number of investigations on the effects of graphene on the mechanical, electrical, and thermal behaviour of polymer based composites have been performed. Ramanathan *et al*. [10] reported the creation of polymeric nanocomposites with functionalized graphene sheets, which overcome obstacles such as the cost of nanoparticles, their availability and good dispersion, and provide superb polymer-particle interactions. Modulus, ultimate strength, and thermal stability follow a similar trend, with values for functionalized graphene sheet-poly(methyl methacrylate) rivalling those for single-walled carbon nanotube-poly(methyl methacrylate) composites. A polystyrene-graphene composite exhibits a percolation threshold of 0.1 volume per cent for room-temperature electrical conductivity, the lowest reported value for any carbon-based composite, except for those involving carbon nanotubes [8]. It has been shown that the thermal conductivity of a graphene/1-octadecanol (stearyl alcohol) nanocomposite increases by nearly 2.5-fold (~140% increase) on addition of ~4 wt.% graphene [11].

As highly-filled polymeric composites, polymer bonded explosives (PBXs) consist of 90-95 wt.% of explosive crystals and 5-10 wt.% of polymeric binder [12-17]. Because of the differences in molecular polarity and structure between explosive crystals and a polymeric binder, PBXs are immiscible, resulting in the inferior performance of the final products. A common and convenient method to improve the interfacial properties of composites is the addition of a bonding or coupling agent [18-21]. It has been found that with the addition of a neutral polymeric bonding agent (NPBA), the interfacial adhesion between the crystals with a fluorinated binder in a 1,3,5,7-tetranitro-1,3,5,7-tetrazocane (HMX)-based PBX is enhanced, leading to improved creep resistant performance and tensile strength [22].

In our previous research [23-25], the addition of graphene improved the mechanical properties and thermal conductivities of PBXs. Hydrogen bonding between 1,3,5-triamino-2,4,6-trinitrobenzene (TATB) and an NPBA in TATB-based PBXs confers a higher mechanical performance on the material [26].

However, the incorporation of graphene and an NPBA into PBXs has been rarely investigated. In the present work, a strategy was designed to improve the mechanical properties of TATB-based PBXs by combining graphene and an NBPA. Creep measurements were performed on the nano-materials in the temperature range 30-80 °C. Furthermore, a six-element mechanical model was used to simulate the creep response of TATB-based PBXs and to analyze the deformation mechanism.

2 Experimental

2.1 Materials

TATB of 98% purity and 17 μm particle size was provided by the Institute of Chemical Materials, CAEP, China. A copolymer of chlorotrifluoroethylene and vinylidene fluoride was used as a polymeric binder, and was obtained from Zhonghao Chenguang Chemical Industry Co., Ltd. China. The raw material graphene, with a specific surface area greater than 500 m^2/g was purchased from Beijing DK Nano Technology Co., Ltd. China, as shown in Figure 1. The length and thickness of the graphene were 1-5 μm and 0.9-1.2 nm, respectively. The properties of the graphene were acquired from the Beijing DK Nano Technology Company. The NPBA, labelled as LBA-02, which was prepared by polymerization from 5,5-dimethylhydantoin as the host material, acrylonitrile (AN) and methyl methacrylate (MMA) as the main monomers, as shown in Equation 1, was obtained from Liming Research Institute of Chemical Industry, China.

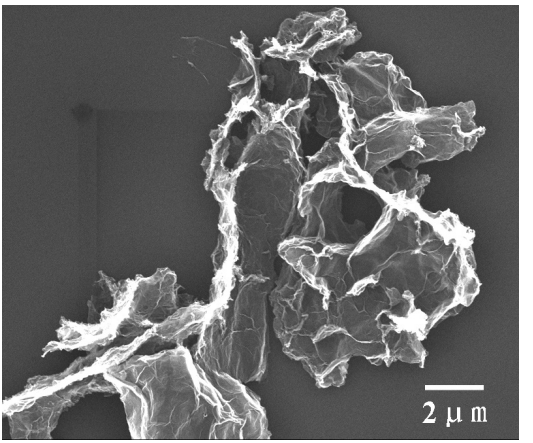

Figure 1. SEM image of graphene

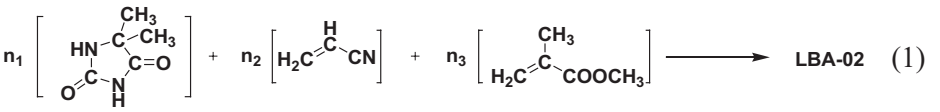

(1)

2.2 Sample preparation

Three formulations were prepared in order to detect the effects of graphene and NPBA, as listed in Table 1. The molding powders of the formulations were produced by a conventional water suspension method. After drying in a vacuum oven at 60 °C for 12 h, the molding powders were pressed in a mold to produce an explosive pellet with the desired geometry.

Table 1. Composition of the TATB-based formulations

Sample	TATB content [wt.%]	Fluoropolymer content [wt.%]	Graphene content [wt.%]	NPBA content [wt.%]
PBX-1	95	5	0	0
PBX-2	95	4.5	0.5	0
PBX-3	95	4.4	0.5	0.1

2.3 X-ray photoelectron energy spectrum (XPS)

A VG 250 X-ray photoelectron energy spectrum obtained with monochromatic Mg-K_a X-rays was used to detect changes of the electron binding energies of elements on the TATB surface.

2.4 Morphology observation

The morphology of the specimens was observed using a scanning electron microscope (SEM; JSM-6390LV, Zeiss) operating at 2.0-20 kV acceleration voltages. The PBX samples were prepared by fracturing the materials during the creep tests. The graphene as received and PBX samples were sputter-coated with a homogeneous gold layer to avoid accumulation of charge.

2.5 Mechanical measurements

The compressive and Brazilian tests were performed with a universal testing machine 5582 (INSTRON, USA) at ambient temperature. Specimens of the explosive pellets, with dimensions of ϕ 20 mm × 20 mm and ϕ 20 mm × 6 mm (diameter × height) were used for the compressive and Brazilian tests. The crosshead speed was set at 0.5 mm/min. A description of the method and

equipment for the Brazilian tests has been given elsewhere [27]. Figure 2 shows a schematic representation of the Brazilian test. Neglecting the contact width, the tensile stress σ in the center could be calculated as [28]:

$$\sigma = \frac{2P}{\pi D\mathrm{t}} \tag{2}$$

where P is the compressive load, D and t are the sample diameter and thickness, respectively.

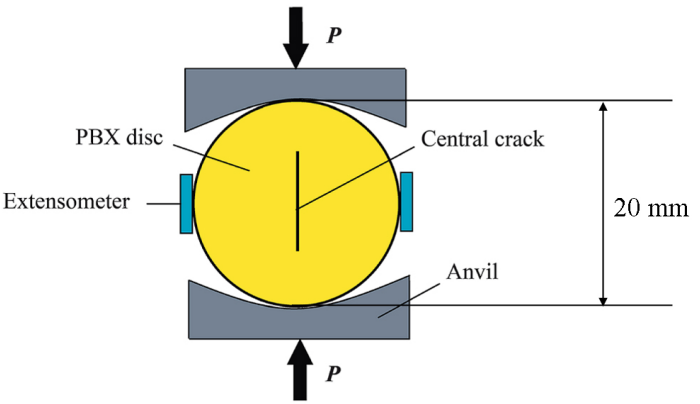

Figure 2. Schematic representation of the Brazilian test

2.6 Dynamic mechanical analysis (DMA) and creep measurements

A DMA 242C apparatus (Netzsch, Germany) was used to conduct dynamic mechanical analyses (DMA) and creep measurements in the three-point bending mode. The specimen with dimensions 30 mm × 10 mm × 1~2 mm (length × width × thickness) was used. During the creep tests, the samples were first heated from room temperature to a set temperature at 3 °C/min, stabilized for 5 min, and then the test, duration 5400 s, was begun under a constant loading stress.

2.7 Sensitivity tests

The impact and friction sensitivity tests were conducted according to GJB-772A-97 standard methods 601.3 and 602.1 [29], using a WL-1 type impact sensitivity instrument and a WM-1 type friction sensitivity instrument, respectively. The conditions for the impact sensitivity tests were: drop weight 5 kg; sample mass 30 mg. The drop height for 50% explosion probability (H_{50})

was used to define the impact sensitivity. In the friction sensitivity test, the relative pressure, pendulum weight, and pendulum angle were set at 3.92 MPa, 1.5 kg, and 90°, respectively, with a sample mass of 30 mg.

2.8 Detonation performance

The detonation heat, detonation pressure, and specific kinetic energy of the TATB-based PBXs were determined according to GJB-772A-97 standard methods 701.1, 704.2 and 705.2 [29], respectively.

3 Six-element Mechanical Model

A six-element mechanical model was successfully used to simulate the creep behaviour of the PBXs [23, 26]. It consisted of consecutively connected one Maxwell and two Kelvin units, as illustrated in Figure 3. The total strain (ε) of the polymeric composite material PBX could be determined by the strains resulting from the Maxwell spring (ε_1), Maxwell dashpot (ε_4), and two Kelvin units (ε_2 and ε_3),

$$\varepsilon(t) = \varepsilon_1 + \varepsilon_2 + \varepsilon_3 + \varepsilon_4 = \frac{\sigma_0}{E_1} + \frac{\sigma_0}{E_2}(1 - e^{-t/\tau_2}) + \frac{\sigma_0}{E_3}(1 - e^{-t/\tau_3}) + \frac{\sigma_0}{\eta_4}t \qquad (3)$$

where $\varepsilon(t)$ denotes a function of creep strain ε with creep time t; σ_0 is the initial stress, E_1 is the elastic modulus of instantaneous elastic deformation, E_2 and E_3 are the elastic moduli of high elastic deformation, τ_2 and τ_3 are the relaxation times, and η_4 is the bulk viscosity, respectively.

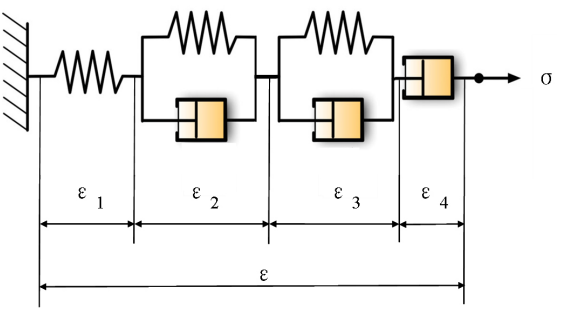

Figure 3. Schematic representation of the six-element mechanical model

4 Results and Discussion

4.1 Surface chemistry analysis

The XPS spectra of TATB surface N 1s and O 1s elements are shown in Figure 4. From the N 1s spectrum of TATB, it can be seen that TATB shows three peaks centered at 397.14 eV, 402.79 eV, and 405.64 eV, respectively. The main peak centered at 397.14 eV corresponds to the nitrogen in the $-NH_2$ groups. Another main peak centered at 402.79 eV and a secondary peak at 405.64 eV belong to nitrogen in the $-NO_2$ groups, in accordance with results reported recently [30]. As illustrated in Figure 4, with the addition of NPBA, the electron binding energies of the N atoms on the nitro-groups of TATB was decreased from 402.79 eV and 405.64 eV to 402.54 eV and 405.49 eV. The electron binding energies of the O atoms on the nitro-groups of TATB decreased from 529.84 eV to 529.69 eV. This weak trend is due to the fact that the NPBA content was very low. However, the decrease trend indicates an electrophilic effect on TATB from the NPBA. Due to the induction effect of the benzene ring, the electron binding energy of N belonging to the amino-groups of TATB also decreased from 397.14 eV to 396.99 eV. The formation of hydrogen bonds between TATB and NPBA is facilitated by the decreasing trend of the electron bonding energy of the oxygen atoms of TATB. The hydrogen atom in the $-CO-NH-$ group of NPBA forms a hydrogen bond with an oxygen atom in the $-NO_2$ group of TATB.

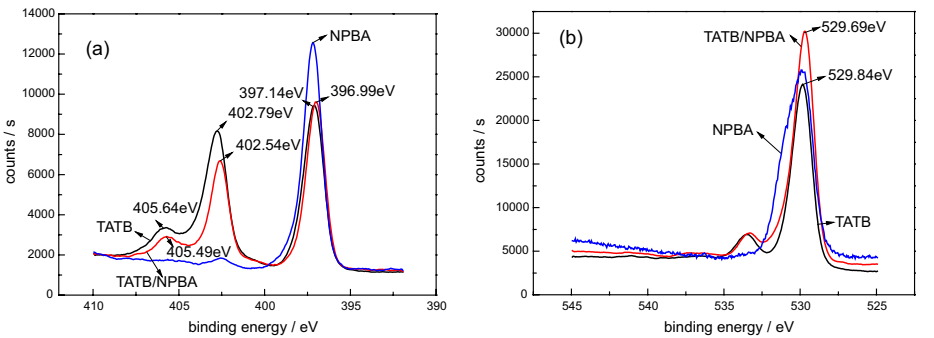

Figure 4. XPS spectra for TATB, NPBA, and TATB/NPBA composites: (a) N 1s, (b) O 1s

4.2 Morphology and characterization

In order to analyze the fracture mechanism, the fracture surfaces in the various materials studied were observed by SEM, as shown in Figure 5. It can be clearly seen that filamentous binder exists at the fracture surface of all of the PBXs,

indicating that binder cleavage is the main rupture mode.

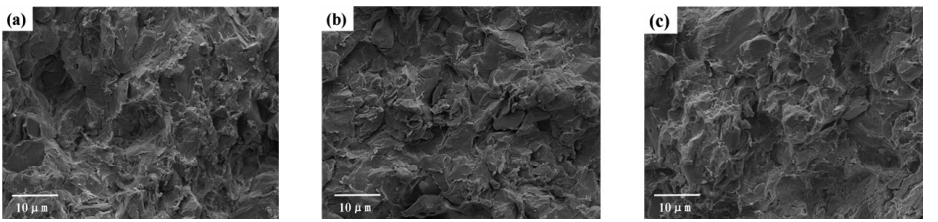

Figure 5. SEM images of fracture surfaces: (a) PBX-1, (b) PBX-2, (c) PBX-3

4.3 Mechanical properties

The DMA data for the materials are presented in Figure 6. It is clear from an inspection of this figure that the storage modulus of raw TATB-based PBXs and its modified composites gradually decreases within the experimental temperature range. These results could be attributed to an energy dissipation phenomenon involving cooperative motions of the polymer chains with temperature [31]. An abrupt decline in the storage modulus curves and a peak in the loss factor curves are observed in the temperature range 40-60 °C, which should be related to a glass transition, when the bulk material ceases to be brittle and glassy in character and becomes less rigid and more rubbery. The storage modulus for PBX-2 with graphene was improved, compared to raw TATB-based PBXs without additives. The storage modulus at 60 °C of the PBXs was increased from 5515 MPa to 5845 MPa on addition of 0.5 wt.% graphene. These results may be related to the fact that graphene restricts the slippage and motion of the polymer chains in the nanocomposite. With the introduction of 0.1 wt.% NPBA, the storage modulus of PBX-3 at 60 °C is further increased to 6331 MPa. This increase may be attributed to the increased interactions between TATB and the polymer chains in the presence of NPBA [26]. The change in loss factor (tanδ) curves is quite small for all three samples.

The results of the compressive and Brazilian tests of the PBXs, conducted at room temperature, are summarized in Table 2. The compressive and tensile strength of the 0.5 wt.% graphene filled PBXs are improved by 5.1% and 29.2%, respectively, compared to the raw TATB-based PBXs without additives. This indicates that the addition of graphene has no significant effect on the compressive mechanical properties but significantly influences the tensile properties. The performance of the composites is further improved by introducing 0.1 wt.% NPBA. It was shown that the PBXs with graphene and NPBA have the highest compressive and tensile strength.

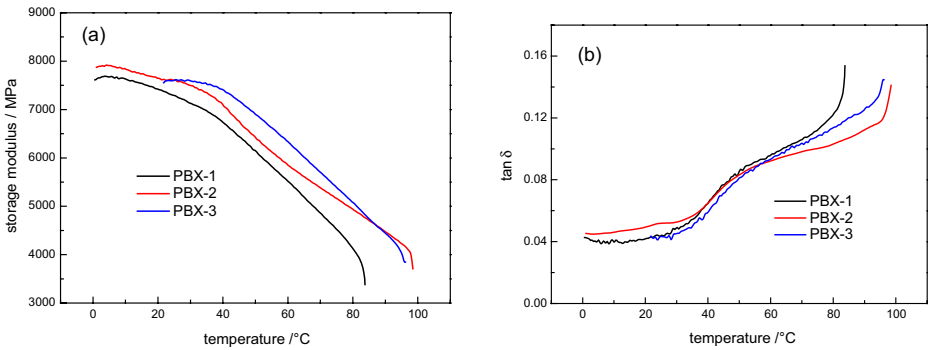

Figure 6. Dynamic mechanical properties for the TATB-based PBXs as a function of temperature: (a) storage modulus, (b) tanδ

Table 2. Mechanical characteristics of the TATB-based PBXs

Sample	Compressive strength [MPa]	Compressive modulus [GPa]	Compressive elongation at cleavage [%]	Tensile strength [MPa]	Tensile modulus [GPa]	Tensile elongation at cleavage [%]
PBX-1	25.81 ±0.19	7.61 ±0.17	1.96 ±0.07	4.76 ±0.05	5.41 ±0.11	0.143 ±0.003
PBX-2	27.12 ±0.21	7.87 ±0.32	2.60 ±0.16	6.15 ±0.20	8.27 ±0.36	0.216 ±0.013
PBX-3	29.21 ±0.26	6.74 ±0.26	2.34 ±0.29	7.10 ±0.08	8.60 ±0.24	0.245 ±0.005

4.4 Three-point bending creep tests

4.4.1 Creep strain curves under different stresses

Three-point bending creep tests were performed with constant stresses of 4 MPa, 7 MPa, and 9 MPa, at an elevated temperature of 60 °C. Figure 7 shows the creep strain versus time for the materials under the three stress levels tested. It may be seen from Figure 7 that at a lower load (4 MPa), no creep rupture was observed for the three-point bending creep process of TATB-based PBXs during the experimental set time (5400 s). PBX-2 filled with graphene deforms significantly less than PBX-1. This improvement in the creep resistance is probably due to the dense and stiff network formed between the nanoparticles and bridging segments, which retards and restricts the mobility of the polymer chains [32]. The smallest creep strain was recorded for PBX-3 with both graphene and NPBA added. The strain at the end of the hold period (after 5400 s) was 40% and 57% smaller for PBX-2 and PBX-3 than for PBX-1. At higher loads (7 MPa and 9 MPa), the three materials responded quite differently. For PBX-1,

the creep strain increased with creep time. The failure of the sample occurred at 4155 s and 660 s under 7 MPa and 9 MPa, respectively. For PBX-2 and PBX-3, no creep rupture times could be obtained under 7 MPa. PBX-2 also exhibited creep failure under 9 MPa. However, PBX-3 displayed a long-term creep process under 9 MPa. The observation that the optimal properties are exhibited in PBX-3 could be also explained by the restricted motion of the chain segments of the polymeric binder by graphene and the increased interactions between TATB and the polymeric binder with NPBA.

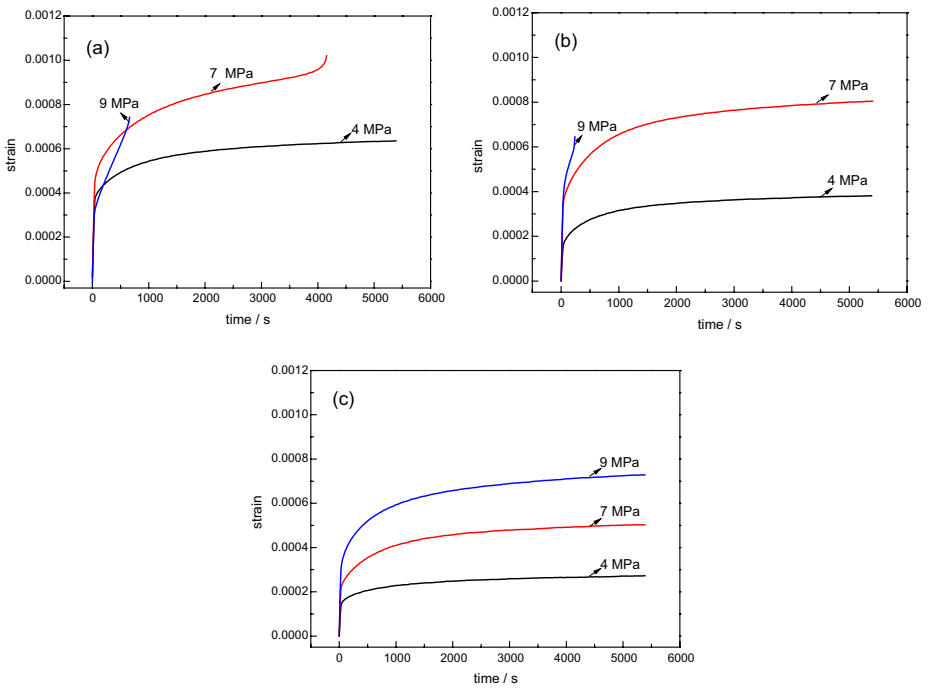

Figure 7. Time-dependent creep strain of the TATB-based PBXs under different stresses at 60 °C: (a) PBX-1, (b) PBX-2, (c) PBX-3

A scheme is proposed to present the microstructure of TATB-based PBXs without and with nano-fillers, as shown in Figure 8. Due to the high aspect ratio, graphene overlaps with itself in the PBXs to construct a three-dimensional network. Because of the appearance of graphene acting as blocking sites, the immobility of the amorphous regions increases. In addition, fairly good interfacial strength between graphene and the polymeric matrix also contributes to the observed enhancement of creep resistance. It may be seen that the NPBA

builds a bridge between TATB and the polymeric binder. One end of the NPBA forms a hydrogen bond with the nitro groups on the surface of the explosive, whilst the other end of the NPBA is entangled with the polymeric binder to enhance the interfacial strength.

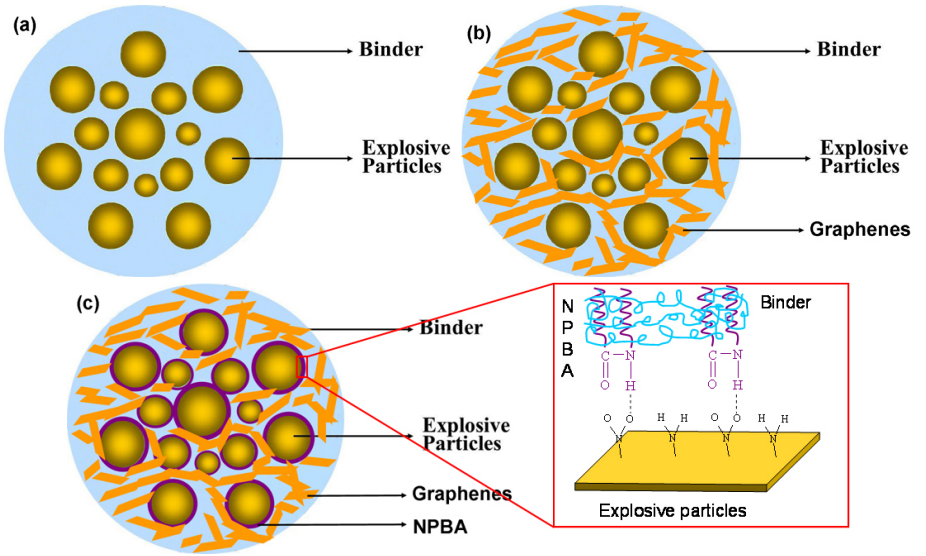

Figure 8. The microstructural schemes in the PBXs: (a) PBX-1, (b) PBX-2, (c) PBX-3

4.4.2 Creep strain curves at different temperatures

Figure 9 shows the dependence of the creep response of the TATB-based PBXs on temperature. The experimental results demonstrated that a prominent increase in the creep strain of the TATB-based PBXs was observed with an increase in temperature. This may be explained by the increased mobility of the polymeric binder at elevated temperatures. At a given temperature, a prominent decrease of the creep strain of PBX-2 was achieved by the addition of 0.5% graphene, compared with PBX-1. The optimal creep resistance was observed for PBX-3.

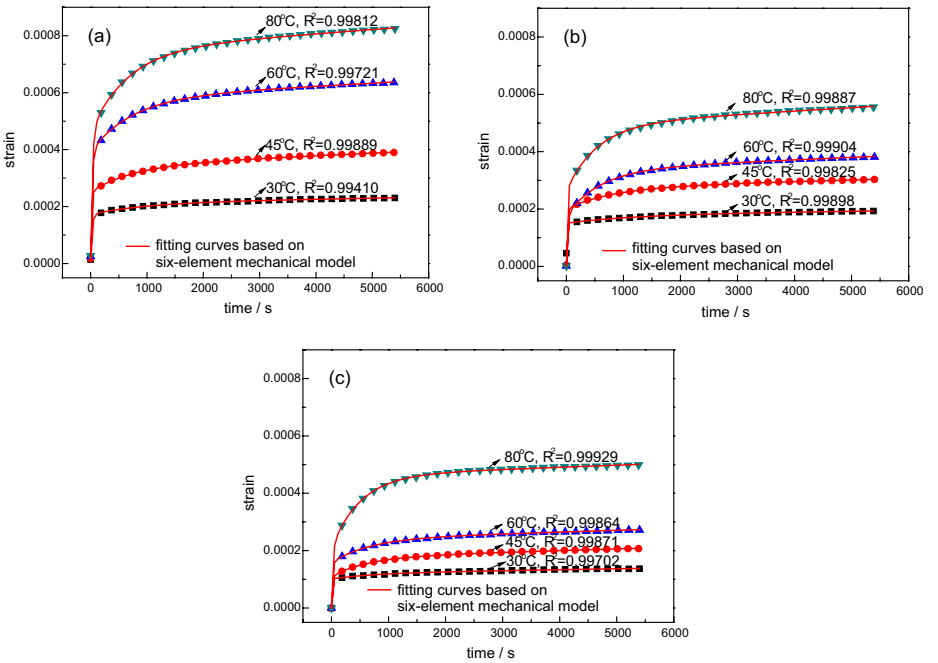

Figure 9. Time-dependent creep strain and fitting results of the TATB-based PBXs at different temperatures at 4 MPa: (a) PBX-1, (b) PBX-2, (c) PBX-3

The steady-state creep strain rate (R_s) was acquired from the slope of the linear fit of the steady-state creep stage of the creep strain curves in Figure 9, as shown in Table 3. It may be seen from Table 3 that R_s gradually increases with temperature. At the same temperature, PBX-1 has the highest value of R_s and PBX-3 has the lowest value of R_s.

Table 3. The steady-state creep strain rate (R_s) of the TATB-based PBXs at different temperatures under 4 MPa

Temperature [°C]	R_s for PBX-1 [s^{-1}]	R_s for PBX-2 [s^{-1}]	R_s for PBX-3 [s^{-1}]
30	4.982×10^{-9}	4.224×10^{-9}	3.707×10^{-9}
45	1.076×10^{-8}	7.279×10^{-9}	6.576×10^{-9}
60	1.397×10^{-8}	9.833×10^{-9}	6.974×10^{-9}
80	1.834×10^{-8}	1.279×10^{-8}	8.100×10^{-9}

4.4.3 Creep fitting

In order to further understand the creep phenomena and mechanism, modelling and prediction of the plots of creep strain versus time using a six-element mechanical model are also presented in Figure 9. The simulated results from the six-element mechanical model agree quite well with the experimental data. The non-linear fitting parameters, including the elastic moduli E_1, E_2, and E_3, the relaxation times τ_2 and τ_3, as well as the bulk viscosity η_4 of the TATB-based PBXs were extracted through direct modelling of the experimental creep data, as shown in Table 4. Based on the parameter analysis of the six-element mechanical model, it may be seen that the values of the elastic moduli E_2 and E_3, and the bulk viscosity η_4 tend to decrease with increasing temperature. Compared with PBX-1 without additives, the parameters E_2, E_3, and η_4 of PBX-2 increase with the addition of graphene particles. PBX-3 exhibits the highest values of E_2, E_3, and η_4. E_2 and E_3 are related to the spring in the Kelvin unit, reflecting the mechanical properties of the amorphous regions [33]. η_4 is associated with the irrecoverable deformation of the materials. The increased values of η_4 indicate the reinforced resistance to viscous flow, which is attributed to the restricted slippage of the polymer chains by graphene and the enhanced particle-matrix bonding by NPBA.

Table 4. The fitting parameters of the six-element model under different conditions

Sample	Test conditions	E_1 [MPa]	E_2 [MPa]	τ_2 [s]	E_3 [MPa]	τ_3 [s]	η_4 [MPa·s]
PBX-1	30°C/4MPa	5.760×10^5	9.999×10^4	974.50	2.419×10^4	25.08	1.150×10^9
	45°C/4MPa	2.720×10^5	4.359×10^4	745.24	1.723×10^4	15.52	4.394×10^8
	60°C/4MPa	4.431×10^5	2.128×10^4	734.98	1.043×10^4	24.82	3.779×10^8
	80°C/4MPa	5.341×10^5	1.403×10^4	665.43	8.773×10^3	28.96	2.727×10^8
PBX-2	30°C/4MPa	8.662×10^4	1.391×10^5	1204.11	3.832×10^4	7.48	1.503×10^9
	45°C/4MPa	1.793×10^6	5.512×10^4	829.95	2.009×10^4	17.20	7.234×10^8
	60°C/4MPa	3.893×10^6	2.525×10^4	606.03	2.248×10^4	23.11	4.661×10^8
	80°C/4MPa	1.011×10^6	1.746×10^4	546.24	1.534×10^4	13.69	3.345×10^8
PBX-3	30°C/4MPa	6.998×10^6	2.084×10^5	772.33	3.964×10^4	7.627	1.240×10^9
	45°C/4MPa	3.465×10^6	6.026×10^4	636.32	2.678×10^4	16.89	6.749×10^8
	60°C/4MPa	4.668×10^6	4.844×10^4	665.66	2.545×10^4	17.66	6.607×10^8
	80°C/4MPa	2.154×10^6	1.578×10^4	506.82	1.940×10^4	22.45	5.508×10^8

4.5 Prediction of long-term creep behaviour

The time-temperature superposition principle (TTSP) [32] was employed to predict the long-term behaviour based on the short-term experimental data. On

the basis of the TTSP theory, a master curve with extended time-scale could be constructed by the horizontal shift of the short-time experimental data at different temperatures. The creep strain curve at a reference temperature T_r and time t_r is received with a horizontal displacement of the creep strain curve at temperature T and time t:

$$\varepsilon(T_r, t_r) = \varepsilon(T_r, t / a_T) = \varepsilon(T, t) \tag{4}$$

where a_T is a shift factor. The constructed master curves of creep strain for the TATB-based PBXs at a reference temperature of 30 °C under 4 MPa are shown in Figure 10. It may be seen that the creep resistance of the nanocomposite with graphene (PBX-2) is obviously enhanced, with a low value of creep strain compared to that of raw PBX-1. PBX-3 with graphene and NPBA incorporated presents the lowest creep strain, suggesting that restricted deformation under the creep process occurs even at an extended time scale.

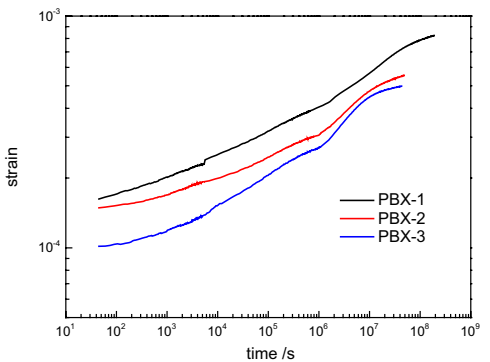

Figure 10. Three-point bending creep strain master curves of the TATB-based PBXs at a reference temperature of 30 °C under 4 MPa

4.6 Sensitivity and detonation performance study

For all of the PBXs, the value of H_{50} was >111.2 cm and the explosion probability (P) was 0%. This indicated that with the addition of graphene and NPBA, the impact and fraction sensitivities remained unchanged.

The results of the detonation performance studies on the PBXs with graphene and NPBA added, are summarized in Table 5. Due to the very small content of graphene and NPBA, no obvious differences between the TATB-based PBXs were observed in their detonation performance.

Table 5. Detonation performance of TATB-based PBXs

Sample	Detonation heat [kJ/g]	Detonation pressure [GPa]	Specific kinetic energy [kJ/g]
PBX-1	4.040	27.3	1.016
PBX-2	3.955	27.2	1.045
PBX-3	3.964	26.5	1.042

5 Conclusions

In summary, the experimental results, fitting and prediction of the long-term creep performance of TATB-based PBXs filled with graphene and NPBA are reported. The experimental results revealed that the non-linear viscoelastic properties of the PBXs were enhanced by the incorporation of graphene and NPBA. The major conclusions from the results in this work are:

(1) The PBXs filled with graphene and NPBA largely surpassed the creep resistance performance of neat PBXs, and was ascribed to the facts that (a) the motion of the surrounding molecular chains was blocked by graphene due to the good interaction between graphene and the polymeric matrix, and (b) the interactions between TATB and the polymeric binder were increased by NPBA.

(2) In order to understand the structure-property relationships, the creep response was fitted by a six-element mechanical model. The variations in the simulated parameters illustrated that graphene and NPBA played a key role in the slippage of the polymeric chains and particle-matrix bonding, resulting in reinforced mechanical properties of the amorphous regions and resistance to viscous flow.

(3) Based on the time-temperature superposition principle, creep strain master curves were obtained at a reference temperature of 30 °C under 4 MPa. The graphene filler and NPBA demonstrated a strongly enhanced effect on the creep resistance of the TATB-based PBXs at an extended long-time scale, which demonstrated the benefit for long-term structure stability and service life of these PBXs.

This work demonstrated the successful application of graphene and NPBA to energetic composites, thereby providing an efficient route for modifying the creep performance of PBXs. The synergistic effect of a nano-filler in a polymeric binder and interfacial modifications will enable researchers to finely enhance the mechanical properties of energetic composites. Thermal conductivity tests that are ongoing for further validating this method, and the influences of the effects

of nano-fillers in polymeric binders and interfacial modifications on thermal conductivity, will be discussed in forthcoming publications.

Acknowledgments
We gratefully acknowledge support from the National Natural Science Foundation of China (51703211, 11402238, 11502243, 11502245, 11702266), the Presidential Foundation of CAEP (No. YZJJLX2016005), and the Science and Technology Fund of CAEP (2015B0101011).

References

[1] Novoselov, K. S.; Geim, A. K.; Morozov, S. V.; Jiang, D.; Zhang, Y.; Dubonos, S. V.; Grigorieva, I. V.; Firsov, A. A. Electric Field Effect in Atomically Thin Carbon Films. *Science* **2004**, *306*: 666-669.
[2] Gong, L.; Yin, B.; Li, L. P.; Yang, M. B. Nylon-6/Graphene Composites Modified Through Polymeric Modification of Graphene. *Composites Part B* **2015**, *73*: 49-56.
[3] Liu, L. Q.; Gao, Y.; Liu, Q.; Kuang, J.; Zhou, D.; Ju, S. T.; Han, B. H.; Zhang, Z. High Mechanical Performance of Layered Graphene Oxide/Poly(vinyl alcohol) Nanocomposite Films. *Small* **2013**, *9*: 2466-2472.
[4] Balandin, A. A. Thermal Properties of Graphene and Nanostructured Carbon Materials. *Nat. Mater.* **2011**, *10*: 569-581.
[5] Gedler, G.; Antunes, M.; Velasco, J. I. Viscoelastic Properties of Polycarbonate-Graphene Nanoplatelets Nanocomposite Foams. *Composites Part B* **2016**, *93*: 143-152.
[6] Wang, H.; Xie, G. Y.; Fang, M. H.; Ying, Z.; Tong, Y.; Zeng, Y. Electrical and Mechanical Properties of Antistatic PVC Films Containing Multi-layer Graphene. *Composites Part B* **2015**, *79*: 444-450.
[7] Ganguli, S.; Roy, A. K.; Anderson, D. P. Improved Thermal Conductivity for Chemically Functionalized Exfoliated Graphite/Epoxy Composites. *Carbon* **2008**, *46*: 806-817.
[8] Stankovich, S.; Dikin, D. A.; Dommett, G. H. B.; Kohlhaas, K. M.; Zimney, E. J.; Stach, E. A.; Piner, R. D.; Nguyen, S. T.; Ruoff, R. S. Graphene-based Composite Materials. *Nature* **2006**, *442*: 282-286.
[9] Molitor, F.; Güttinger, J.; Stampfer, C.; Dröscher, S.; Jacobsen, A.; Ihn, T.; Ensslin, K. Electronic Properties of Graphene Nanostructures. *J. Phys: Condens. Matter* **2011**, *23*: 243201.
[10] Ramanathan, T.; Abdala, A. A.; Stankovich, S.; Dikin, D. A.; Herrera-Alnso, M.; Piner, R. D.; Adamson, D. H.; Schniepp, H. C.; Chen, X.; Ruoff, R. S.; Nguyen, S. T.; Aksay, I. A.; Prud'homme, R. K.; Brinson, L. C. Functionalized Graphene Sheets for Polymer Nanocomposites. *Nat. Nanotechnol.* **2008**, *3*: 327-331.
[11] Yavari, F.; Fard, H. R.; Pashayi, K.; Rafiee, M. A.; Zamiri, A.; Yu, Z. Z.;

Ozisik, R.; Borca-Tasciuc, T.; Koratkar, N. Enhanced Thermal Conductivity in a Nanostructured Phase Change Composite Due to Low Concentration Graphene Additives. *J. Phys. Chem. C* **2011**, *115*: 8753-8758.

[12] Qiao, Z. Q.; Shen, J. P.; Wang, J.; Huang, B.; Yang, Z. J.; Yang, G. C.; Zhang, K. L. Fast Deflagration to Detonation Transition of Energetic Material Based on a Quasi-Core/Shell Structured Nanothermite Composite. *Compos. Sci. Technol.* **2015**, *107*: 113-119.

[13] Hobbs, M. L.; Kaneshige, M. J. Ignition Experiments and Models of a Plastic Bonded Explosive (PBX 9502). *J. Chem. Phys.* **2014**, *140*: 124203.

[14] Li, T.; Hua, C.; Li, Q. Shock Sensitivity of Pressed RDX-based Plastic Bonded Explosives under Short-duration and High-pressure Impact Tests. *Propellants Explos. Pyrotech.* **2013**, *38*: 770-774.

[15] Vadhe, P. P.; Manickam, S.; Rahujade, N.; Kondra, A.; Prasad, U.; Sinha, R. K. Studies on Tungsten Based High Density Cast Polymer Bonded Explosive (PBX) Formulations. *Cent. Eur. J. Energ. Mater.* **2015**, *12*: 497-506.

[16] He, G. S.; Yang, Z. J.; Zhou, X. Y.; Zhang, J. H.; Pan, L. P.; Liu, S. J. Polymer Bonded Explosives (PBXs) with Reduced Thermal Stress and Sensitivity by Thermal Conductivity Enhancement with Graphene Nanoplatelets. *Compos. Sci. Technol.* **2016**, *131*: 22-31.

[17] Kaur, J.; Arya, V. P.; Kaur, G.; Lata, P. Evaluation of the Thermo-Mechanical and Explosive Properties of Bimodal and Hybrid Polymer Bonded Explosive (PBX) Compositions Based on HNS and HMX. *Cent. Eur. J. Energ. Mater.* **2013**, *10*: 371-392.

[18] Kabir, M. M.; Wang, H.; Lau, K. T.; Cardona, F. Chemical Treatments on Plant-based Natural Fibre Reinforced Polymer Composite: an Overview. *Composites Part B* **2012**, *43*: 2883-2892.

[19] Li, F.; Ye, L.; Nie, F. D.; Liu, Y. G. Synthesis of Boron-containing Coupling Agents and its Effect on the Interfacial Bonding of Fluoropolymer/TATB Composite. *J. Appl. Polym. Sci.* **2007**, *105*: 777-782.

[20] Liu, Y. F.; Chen, Y.; Shi, L.; Yao, W. S. Synthesis of Three Novel Laurylamine-derived Long-chain Alkyl Bonding Agents and Their Interactions with RDX. *Propellants Explos. Pyrotech.* **2012**, *37*: 69-76.

[21] John, M. J.; Tlili, R.; Anandjiwala, R. D.; Boudenne, A.; Ibos, L. Effect of Amphiphilic Coupling Agent on Heat Flow and Dielectric Properties of Flax-Polypropylene Composites. *Composites Part B* **2012**, *43*: 526-532.

[22] Liu, J. H.; Liu, S. J.; Chen, L. L.; Lin, C. M.; Gong, F. Y.; Nie, F. D. Improving Mechanical Property of HMX-based PBX with Neutral Polymer Bonding Agent. *Int. Annu. Conf. ICT, 45th*, Karlsruhe, Germany **2014**, 56/1-8.

[23] Lin, C. M.; He, G. S.; Liu, J. H.; Huang, Z.; Pan, L. P.; Zhang, J. H.; Liu, S. J. Enhanced Non-linear Viscoelastic Properties of TATB-based Polymer Bonded Explosives Filled with Hybrid Graphene/Multiwalled Carbon Nanotubes. *RSC Adv.* **2015**, *5*: 94759-94767.

[24] Lin, C. M.; He, G. S.; Liu, J. H.; Liu, S. J. Improved Thermal Conductivity for

TATB-based Polymer Bonded Explosives with Graphene Nanoplatelets. *Int. Autumn Seminar on Propellants, Explosives and Pyrotechnics, 6th*, Qingdao, China, 2015, 402-406.

[25] Lin, C. M.; He, G. S.; Liu, J. H.; Pan, L. P.; Liu, S. J. Construction and Thermal Properties of Nanostructured Polymer Bonded Explosives with Graphene. *RSC Adv*. **2015**, *5*: 98514-98521.

[26] Lin, C. M.; Liu, J. H.; He, G. S.; Chen, L. L.; Huang, Z.; Gong, F. Y.; Liu, Y. G.; Liu, S. J. Non-linear Viscoelastic Properties of TATB-based Polymer Bonded Explosives Modified by a Neutral Polymeric Bonding Agent. *RSC Adv.* **2015**, *5*: 35811-35820.

[27] Wen, M. P.; Tang, W.; Zhou, X. Y.; Pang, H. Y.; Zhu, F. Y. Tensile Mechanical Properties of Brittle Explosives Evaluated by Arc Compress Head Brazilian Test. *Chinese J. Energ. Mater.* **2013**, *21*: 490-494.

[28] Chen, P. W.; Huang, F. L.; Ding, Y. S. Microstructure, Deformation and Failure of Polymer Bonded Explosives. *J. Mater. Sci.* **2007**, *42*: 5272-5280.

[29] *National Military Standard of China, Experimental Methods of Sensitivity and Safety* (in Chinese), GJB-772A-97, **1997**.

[30] Carter, J. A.; Zaug, J. M.; Nelson, A. J.; Armstrong, M. R.; Manaa, M. R. Ultrafast Shock Compression and Shock-induced Decomposition of 1,3,5-Triamino-2,4,6-trinitrobenzene Subjected to a Subnanosecond-duration Shock: an Analysis of Decomposition Products. *J. Phys. Chem. A* **2012**, *116*: 4851-4859.

[31] Feng, Q. P.; Shen, X. J.; Yang, J. P.; Fu, S. Y.; Mai, Y. W.; Friedrich, K. Synthesis of Epoxy Composites with High Carbon Nanotube Loading and Effects of Tubular and Wavy Morphology on Composite Strength and Modulus. *Polymer* **2011**, *52*: 6037-6045.

[32] Yang, J. L.; Zhang, Z.; Schlarb, A. K.; Friedrich, K. On the Characterization of Tensile Creep Resistance of Polyamide 66 Nanocomposites, Part II: Modeling and Prediction of Long-term Performance. *Polymer* **2006**, *47*: 6745-6758.

[33] Li, Y. Z.; Kessler, M. R. Creep-resistant Behavior of Self-reinforcing Liquid Crystalline Epoxy Resins. *Polymer* **2014**, *55*: 2021-2027.